https://doi.org/10.48048/tis.2022.3046

The Electromagnetic Interference Shielding Effectiveness and Dielectric Response of PVDF-nTiO$_2$Nanocomposites Thin Films

Santhoshkumar Dani[1], Prachalith Nagaleekara Channabasavanna[1], Sudheendra Kulkarni[2], Shambonahalli Rajanna Manohara[3] and Khadke Udayakumar[1,*]

[1]Department of Physics, Vijayanagara Sri Krishnadevaraya University, Ballari 583105, India
[2]Department of Physics, KLS Gogte Institute of Technology, Belagavi 590006, India
[3]Nano-Composites and Materials Research Lab, Department of Physics, SiddagangaInstitute of Technology,Tumakuru 572103, India

([*]Corresponding author's e-mail: khadke@vskub.ac.in)

Received: 13 March 2022, Revised: 26 April 2022, Accepted: 13 May 2022, Published: 1 November 2022

Abstract

This paper presents electromagnetic interference (EMI) shielding effectiveness (SE) and dielectric response of Polyvinylidene Fluoride (PVDF) and PVDF-Titanium dioxide (nTiO$_2$) nanocomposite thin films. nTiO$_2$ nanoparticles were synthesized by the combustion method using urea as fuel. PVDF and PVDF-nTiO$_2$nanocomposite thin films of different wt% of TiO$_2$as fillers in the PVDF matrix were prepared using the solvent evaporation method. The synthesized nanocomposite thin films were characterized by XRD, FTIR, and SEM. The EMI-SE was studied in the frequency range 0.5 - 8GHz and dielectric response in 10Hz - 8MHz at room temperature. The EMI-SE shows up and down valleys in S-Band with an average variation of ~28 and ~35 dB at 2 and 4GHz respectively and remains stable in C- Band agreeing with existing literature. The dielectric constant of PVDF-nTiO$_2$ nanocomposite thin films decreases with an increase in frequency and anomaly for 10wt% of nTiO$_2$ fillers in the PVDF matrix at standard frequency.

Keywords: Ferroelectric polymer, PVDF-nTiO$_2$, EMI shielding, Dielectric constant, Thin films, Nanocomposite

Introduction

In today's life, the use of electronic devices has increased enormously which absorb and radiate electromagnetic waves affecting the performance of associated electronic circuits. Most of the electromagnetic radiation absorbed by the human body leads to different health issues [1,2]. To minimize these issues arising due to EMI, effective shielding materials need to protect the efficient operation of electronic systems. Electromagnetic interference (EMI) shielding is defined as the attenuation of the propagating electromagnetic waves produced by the shielding material [3]. The EMI-SE is based on 3 working principles viz, reflection, multiple reflections, and absorption [4]. For reflection, the material should exhibit conducting properties with mobile charge carriers and for absorption, the material should contain magnetic and/or electric diploes to produce a high dielectric constant for shielding effect under electromagnetic irradiation.

The Effective EMI SE can be calculated by the formula;

$$EMISE = 10log\frac{P_I}{P_T} = 10log\frac{1}{T} \quad (1)$$

where P_I and P_T represent the power of incident and transmitted wave respectively and for non-shielding materials P_I and P_T are Eq. (1). The total EMI SE (SE_{Total}) in a material is a consequence of absorption (SE_A), reflection (SE_R), and multiple reflections (SE_M) as represented by the equation;

$$SE_{Total} = SE_A + SE_R + SE_M \quad (2)$$

The SE_M is usually neglected when the total SE is beyond 10 dB and depends only on SE_A and SE_R. The SE_A loss occurs due to currents induced in the medium to produce ohmic losses and heating of the material. It increases with an increase in frequency. Good absorbing material possesses high conductivity

and sufficient permeability to achieve the required number of skin depths in the material even at the lowest frequency. SE_R is related to the relative impedance mismatch between the shielding surface and propagating wave. It is also determined in terms of a ratio of conductivity and permeability of shielding material and it decreases with increasing frequency. Finally, the SE_M occurs due to multiple reflections of the already reflected waves at the boundary. The multiple internal losses occur due to porous material structure and are related to absorption loss [5].

One of the established solutions in the elimination of EMI is the optimized use of lossy dielectric materials and magnetic materials as they shield the electronic devices from unwanted EM radiation by absorption and reflection. Generally, absorption dominant shielding materials are suitable for devices rather than reflection, since reflection again may lead to further interference effects to nearby devices. So the good absorbing material should possess the criteria of thin, lightweight, less dense, wide-range frequency bandwidth, and robust absorption capability [6]. It should also exhibit a high dielectric constant. Because of the high dielectric constant, the absorption loss may take place due to the polarization of electric and magnetic dipoles moment inside the material [7].

PVDF is a semi-crystalline polymer with different crystalline forms [8] that has attracted many researchers as it possesses simple chemical formula $-CH_2-CF_2-$ and exhibits a variety of characteristics such as mechanical, electrical properties, non-linear optical properties, memory devices, photovoltaic applications, and battery applications. The application of a high electric field produces the polarization of the PVDF film due to the alignment of hydrogen and fluorine ions according to their respective electrical polarities. The formation of these aligned dipoles can account quite well for the observed piezoelectric and pyroelectric behavior of this polymer [9].

The β phase PVDF was widely investigated for its interesting properties of pyro-, piezo-, and ferroelectricity and its inherent properties of lightweight, mechanical flexibility, and easy processing [10]. However, it has a high dielectric constant but there are no reports on the use of PVDF-based $nTiO_2$ nanocomposites thin film for EMI-SE.

This paper describes the preparation and characterization techniques of PVDF-$nTiO_2$ nanocomposite thin films. The EMI-SE and dielectric properties of these composites measured as a function of frequency were reported.

Materials and methods

PVDF granules with a molecular weight of 534,000 were procured from Sigma Aldrich, India. To synthesize TiO_2 nanoparticles, we used AR-grade bulk TiO_2 procured from SD fine-chem. Ltd. Mumbai, India, Urea by Fisher Scientific India Pvt. Ltd., Mumbai, and N N-Dimethylacetamide (DMAC) used as solvent was procured from Spectrochem Pvt. Ltd., Mumbai, India.

Preparation of $nTiO_2$nanoparticles

A known quantity of solid urea used as fuel was ground for 20 min and added to a known quantity of bulk TiO_2 and mixed well. The combustion process was then performed on a hot plate at about 300 °C for 10 min. The produced yellowish precursor was grounded and calcined in a muffle furnace at 500 °C for an hour to give white color TiO_2 nanoparticles [11]. **Figure 1** shows the flowchart representing the steps of the combustion method used to prepare $nTiO_2$ nanoparticles.

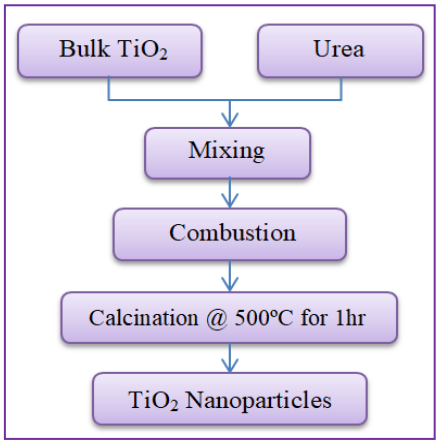

Figure 1 Flowchart representation of combustion method.

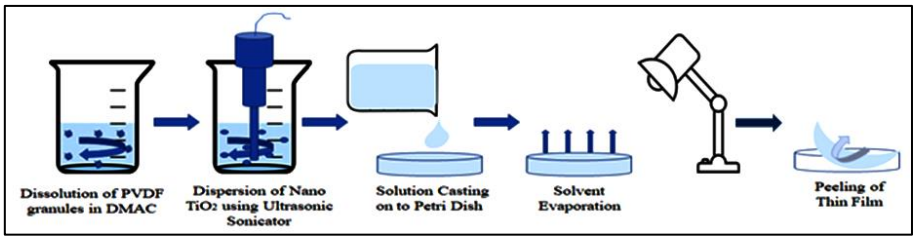

Figure 2 Solvent evaporation technique.

Preparation of PVDF and PVDF-nTiO$_2$nanocomposite thin films

Pristine PVDF and PVDF- nTiO$_2$ composite thin films were blended by a simple solution mixing method. 3gm of PVDF granules was dissolved in 30 mL of DMAC solvent and heat-treated at 50 °C using a magnetic stirrer to get a homogenous solution [12]. A standardized PVDF- nTiO$_2$ solution was obtained by adding nTiO$_2$ particles in the wt% ratio of 2, 4, 6, 8, and 10 % into the PVDF solution. To uniformly disperse the particles in the polymer matrix, the solution was sonicated for an hour and the solution was poured into the petri dish and placed under an incandescent bulb (40 Watt) for 2- 4 h so that the solvent gets completely evaporated. After drying, the PVDF film was peeled-off from the petri dish as shown in **Figure 2**. The prepared PVDF-nTiO2 nanocomposite thin films are flexible with thicknesses ranging between 140 - 150 µm and were used for further studies.

Results and discussions

XRD Analysis

The X-ray diffraction study was carried out using Bruker, AXS D8 Advance X-ray diffractometer using Cu-Kα radiation (λ) = 1.5418 Å and data recorded for the 2θ ranging from 5 - 90 ° with steps 0.2107 °. **Figures3** and **4** show the XRD pattern of the synthesized nTiO$_2$ nanoparticles and PVDF -nTiO$_2$ nanocomposites of different wt.% of nTiO$_2$ in PVDF respectively. From **Figure 3**, it is observed that the 2θ peaks at 25.33 ° (101), 36.98 ° (103), 37.81 ° (004), 38.61 ° (112), 48.10 ° (200), 53.92 ° (105), 55.13 ° (211), 62.18 ° (213) and 62.75 ° (204) defines the TiO$_2$anatase structure.The size of the nanoparticles was found to be 59.13nm estimated using the Debye-Scherer Eqs. (13) - (16). In **Figure 4**, the 2θ peaks at 18.46 °(020) and 20.16 °(110) confirm the presence of α and β phases of pure PVDF. An increase in the intensity of prominent peaks of nTiO$_2$ particles is observed when the concentration of the composition varies from 2 - 10 wt.%. The peak value corresponding to β-phase PVDF remains prominent at 2θ= 20.16 ° and there is no observed shift in peak as nTiO$_2$ particles are immersed but intensity drops abruptly at 10 wt.% of nTiO$_2$ in PVDF. The crystallinity of the composites is enhanced due to the formation of cationic complexes with the functional group of PVDF, which confirms the intercalation of nTiO$_2$ with the PVDF polymer system.

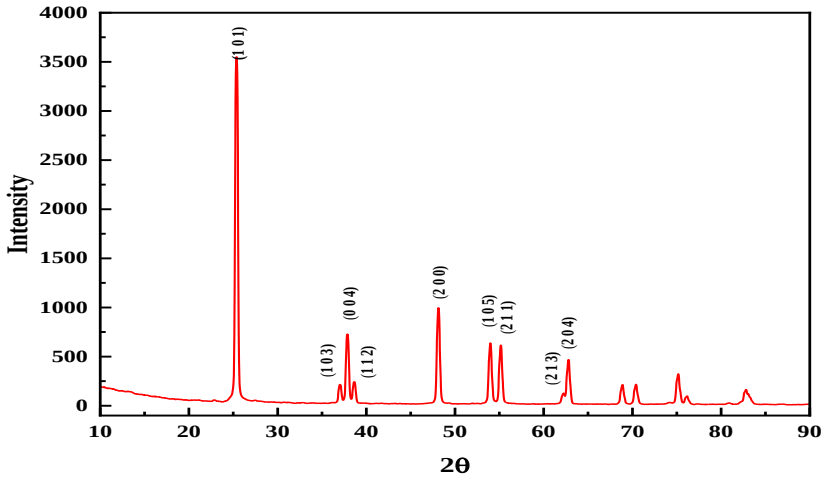

Figure 3 XRD pattern of nTiO$_2$.

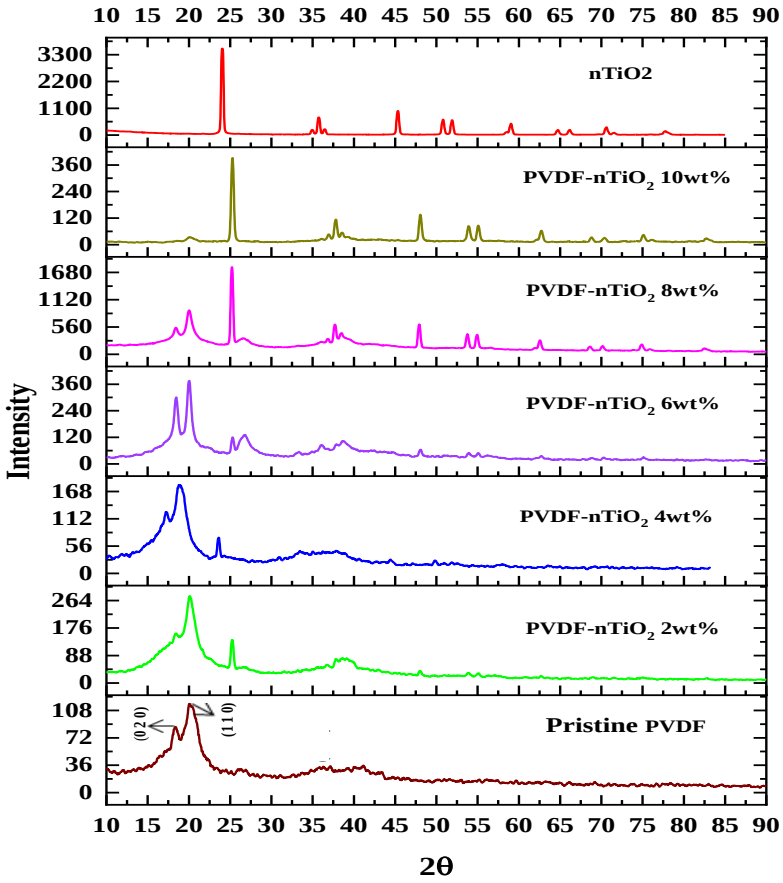

Figure 4 XRD pattern of pristine PVDF, $nTiO_2$ and PVDF-$nTiO_2$ composites.

FTIR spectra analyses

Fourier transform infrared spectrophotometer (Perkin Elmer Spectrum Two L160000U) was used to study bonding interactions in the nanocomposite of varied filler concentrations in the wavelength range between 400 - 4,000 cm^{-1}. **Figure 5** shows a strong absorption band corresponding to the unequal and equal stretching vibrations of the CH_2 group in the PVDF matrix observed at 3,025 and 2,985 cm^{-1}. The region 1,450 to 1,000 cm^{-1} represents the continuous band absorption region which corresponds to fluorocarbon absorption (C - F). The entire characteristic vibrational bands (480, 510,840, 882, 1,071, 1,401 cm^{-1}) are in agreement with existing literature [17,18]. This shows that the PVDF is of β-form in the polymer matrix. This report is in agreement with XRD results. The broadest band is observed at 3,500 cm^{-1}, corresponding to the stretching vibration of the hydroxyl group O-H of the $nTiO_2$ nanoparticles. The band observed around 1,630 cm^{-1}, corresponding to bending modes of Ti-OH; the prominent peak at 1,383 cm^{-1} related to Ti-O modes [4,17,18].

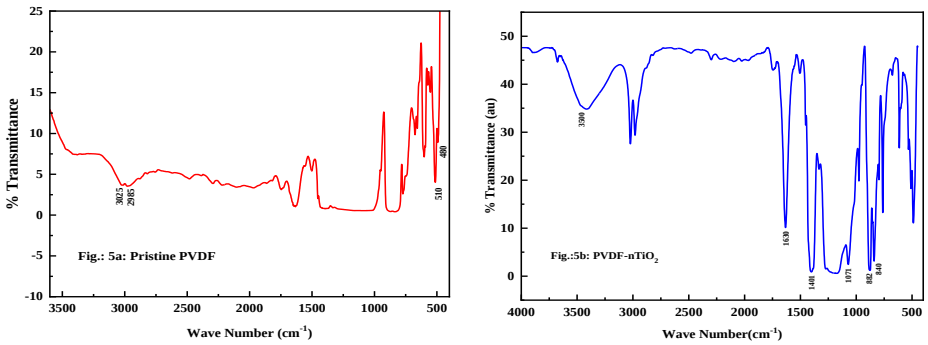

Figure 5 FTIR spectra of a) Pristine PVDF, and b) PVDF-$nTiO_2$.

SEM micrographs analysis

Surface morphology was recorded using a scanning electron microscope (Carle Zeiss Pvt Ltd, Germany; model: EVO 18). SEM images of pristine PVDF, $nTiO_2$ particles, PVDF-$nTiO_2$ (6wt%) and PVDF-$nTiO_2$ (10wt%) are shown in **Figures 6(a) - 6(d)**, respectively. **Figures 6(c)** and **6(d)** exhibit uniform distribution of $nTiO_2$ particles in the PVDF matrix. The images show the variation of pore size with 2 different wt% (6 and 10) of $nTiO_2$ in the PVDF matrix i.e. size of the pores condenses as the $nTiO_2$ particles start occupying the pores. This represents, that the addition of $nTiO_2$ in the PVDF matrix increases the structural density and affects the surface morphology of the composite films which leads to the variation of dependent parameters of different properties of PVDF nanocomposite thin films.

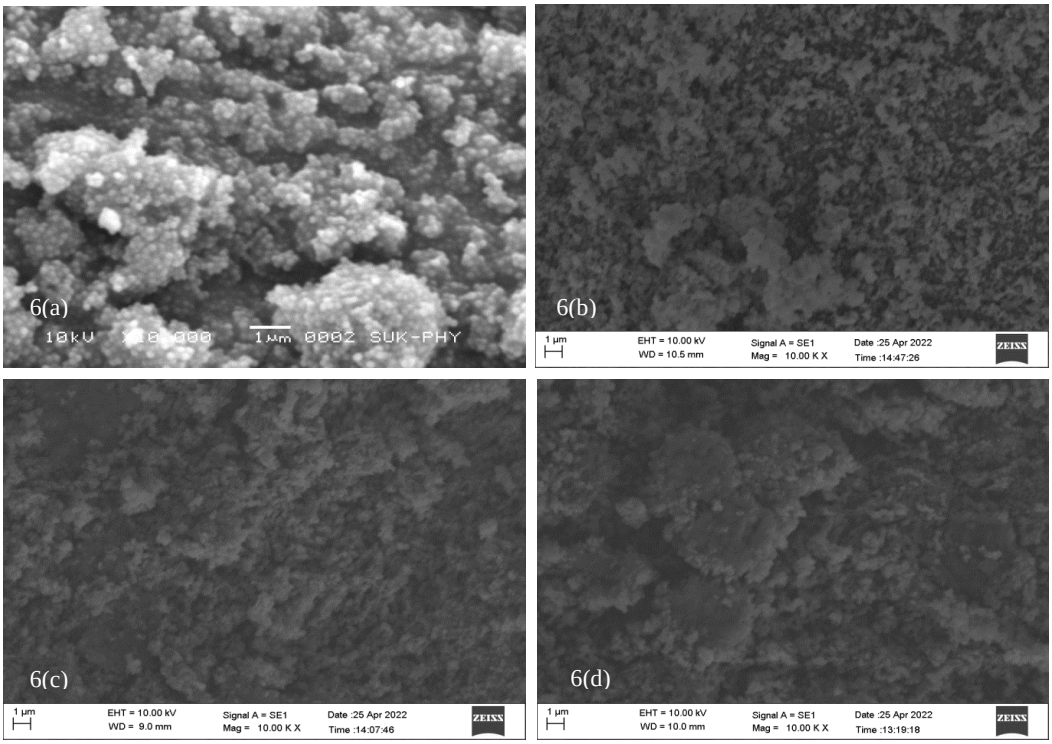

Figure 6 SEM images of a) pristine PVDF, b) $nTiO_2$,c) PVDF-$nTiO_2$ (6wt%), and d) PVDF-$nTiO_2$ (10wt%).

EMI-shielding effectiveness studies

The EMI shielding effectiveness (EMI-SE) of the prepared nanocomposite thin films was measured using Vector Network Analyzer (Copper Mountain Technologies, USA; model: 804/1) in the frequency range between 300 kHz - 8 GHz. The EMI-SE of PVDF and PVDF-TiO_2 nanocomposite thin films for frequency and different wt% for selected frequencies are shown in **Figures 7** and **8** respectively. The EMI-SE of PVDF-$nTiO_2$ nanocomposite films is dependent on frequency mainly due to absorption. On incorporation of $nTiO_2$ in the PVDF matrix, the EMI shielding value increases to a maximum of 35.31 dB at a frequency of 4.58 GHz for 2wt%. The increase in wt% of the nanoparticles to the PVDF matrix has varied the EMI shielding of nanocomposite thin films. The EMI-SE shows up and down valleys in S-Band(in the range 2-4GHz) with an average variation of ~28 and ~35% around 2 and 4GHz respectively and stable in C- Band(4-8GHz) agreeing with existing literature [19,20]. Further, the results show the decreasing trend of EMI-SE with an increase in wt% of $nTiO_2$ fillers in the PVDF matrix due to frozen in polarization.

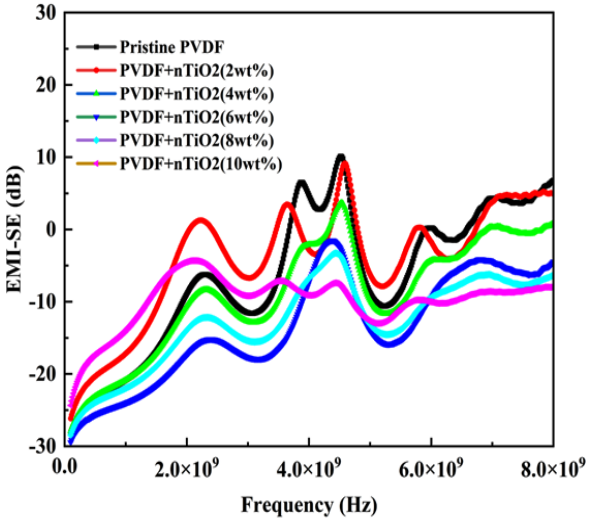

Figure 7 Variation of EMI-SE with Frequency for PVDF and $nTiO_2$ composites.

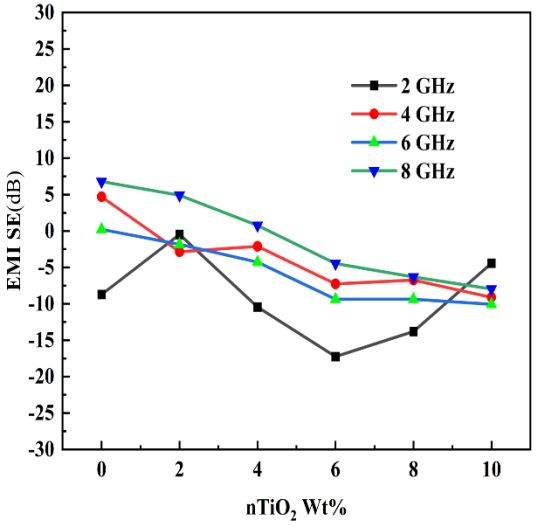

Figure 8 Variation of EMI-SE with Wt% for different frequencies.

Dielectric studies

The dielectric constant and dielectric loss of the prepared PVDF nanocomposite thin films were estimated [21] using the values of parallel capacitance measured using an LCR meter (HIOKI Japan, model-IM3536) in the frequency range between 50 Hz - 8 MHz at room temperature. **Figures 9** and **10** show the variation of dielectric constant and dielectric loss for pristine PVDF, and PVDF-$nTiO_2$ (2, 4, 6, 8, and 10 wt%) nanocomposite thin films with frequency respectively. The dielectric constant of all PVDF-$nTiO_2$ nanocomposite thin films decreases with an increase in frequency in the range between 50 Hz - 8MHz (in VLF to ~HF range). At low frequency (< 100 Hz) the dielectric constant increases with an increase in wt% of $nTiO_2$ in the PVDF matrix and anomaly at 10 wt% of $nTiO_2$ fillers and later remains constant at a higher frequency. The increase in the dielectric constant of PVDF-$nTiO_2$ (10wt%) is due to the collective effect and harmonization of space charge polarisation due to uniform dispersion of $nTiO_2$ in PVDF as depicted in the SEM micrograph (**Figures 6(c)** and **6(d)**). Whereas the decrease in the dielectric constant at higher frequencies is contributed to the increase in the density of the dipoles and that may hinder the orientation polarization. The dielectric loss plots follow similar behavior as that of the dielectric constant without any correlation with filler composition. The dielectric loss decreases in the low-frequency region and follows a downward falling trend in the high-frequency region. Thus, the broadband dielectric measurements provided evidence of interfacial polarization in the thin films, and the decrease in the dielectric constant with increasing frequency is due to the constraints of orientation polarization, which confirmed the dipole-dipole interaction in hybrid polymer PVDF-$nTiO_2$ nanocomposite thin films.

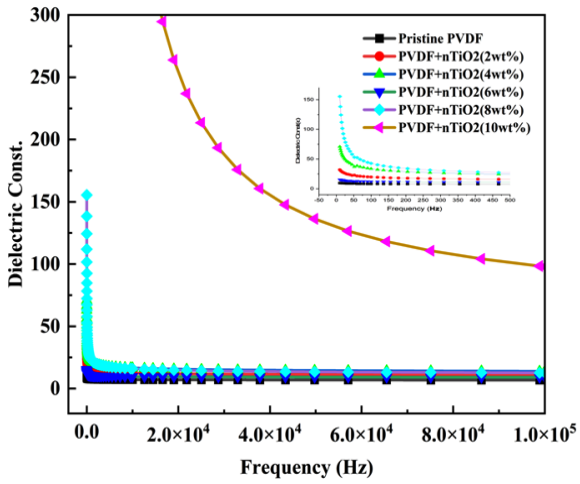

Figure 9 Variation of dielectric constant with frequency for PVDF and $nTiO_2$ composites.

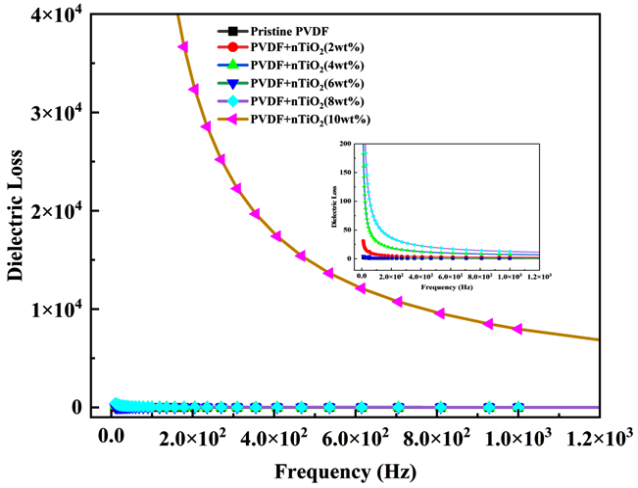

Figure 10 Variation of dielectric loss with frequency for PVDF and $nTiO_2$ composites.

Conclusions

PVDF and PVDF-TiO_2 nanocomposite thin films of different stoichiometric ratios were prepared by a simple solvent evaporation method. XRD and SEM confirm the uniform dispersion of $nTiO_2$ fillers in the PVDF matrix. The size of the synthesized $nTiO_2$ nanoparticles is 59.14nm and β-phase confirmation of PVDF and $nTiO_2$ in the anatase phase. The Uniform dispersion of nanofillers that increases the structural density is depicted by an SEM micrograph. FTIR spectrum confirmed the chemical composition of the thin films. The incorporation of nanoparticles in the PVDF matrix enhanced the dielectric properties with the dielectric constant of 155.437 for 8wt% and 152,450.12 an anomaly at 10wt% with minimum dielectric loss. The incorporation of nanofillers also resulted in a higher EMI-SE of 27.42 dB at 2.2 GHz and 35.31 dB at 4.58 GHz for 2wt%. A wide range of frequency band dielectric spectroscopy and EMI-SE measurements provided evidence of interfacial polarization in the films, and the decrease in the dielectric constant with increasing frequency is associated with restrictions on orientation polarization, which confirms the presence of dipoles in hybrid composite films that forms a better EMI-SE material.

Acknowledgments

One of the authors gratefully acknowledges the financial support from Inter-University Accelerator Centre (IUAC), New Delhi, under Project No. UFR-70320. The authors are also thankful to Miss Bibi Raza Khanam, Department of Physics, Vijayanagara Sri Krishnadevaraya University Ballari, Karnataka, India for their support to the completion of this work.

References

[1] LY Matzui, OA Syvolozhskyi, LL Vovchenko, OS Yakovenko, OA Lazarenko, TA Len, OV Ischenko, AG Dyachenko, AV Vakaliuk, VV Oliynyk and VV Zagorodnii. Electrical and electromagnetic interference shielding properties of GNP-NiFe hybrid composite with segregate structure of conductive networks. *J. Appl. Phys.* 2022; **131**, 055110.

[2] M Cao, XX Wang, W Cao, XY Fang, B Wen and J Yuan. Thermally driven transport and relaxation switching self-powered electromagnetic energy conversion. *Small* 2018; **14**, 1800987.

[3] M Zahid, HMF Shakir and ZA Rehan. Electromagnetic interference shielding study in microwave and NIR regions by highly efficient Ag/ZnS and polyaniline-Ag/ZnS particles. *J. Thermoplastic Compos. Mater.* 2021, https://doi.org/10.1177/08927057211064990.

[4] A León, P Reuquen, C Garín, R Segura, P Vargas, P Zapata and PA Orihuela. FTIR and Raman Characterization of TiO_2 nanoparticles coated with polyethylene glycol as carrier for 2-methoxyestradiol. *Appl. Sci.* 2017; **7**, 49.

[5] M Oh, Y Yoon, E Jang and D Moon. Study of dielectric and thermal conductivity characteristics of polyimide composite. *Mater. Sci. Appl.* 2019; **10**, 197-204.

[6] N Maruthi, M Faisal and N Raghavendra. Conducting polymer-based composites as efficient EMI shielding materials: A comprehensive review and future prospects. *Synthetic Met.* 2021; **272**, 116664.

[7] S Sankaran, K Deshmukh, MB Ahamed, KK Sadasivuni, M Faisal and SKK Pasha. Electrical and Electromagnetic Interference (EMI) shielding properties of hexagonal boron nitride nanoparticles reinforced polyvinylidene fluoride nanocomposite films. *Polymer Plast. Tech. Mater.* 2019; **58**, 1191-209.

[8] RL Fleischer, PB Price andRM Walkaer. *Nuclear tracks in solids: Principles and applications*. University of California Press, California, 1975.

[9] R Spohr. *Ion tracks and microtechnology: Basic principles and applications*. Vieweg, Braunschweig, Germany, 1990.

[10] L Ruan, XN Yao, YF Chang, LQ Zho, GW Qin and XM Zhang. Properties and applications of the β phase poly(vinylidene fluoride). *Polymers* 2018; **10**, 228.

[11] MY Nassar, EI Alia and ES Zakaria. Tunable auto-combustion preparation of TiO_2 nanostructures as efficient adsorbents for the removal of an anionic textile dye. *RSC Adv.* 2017; **7**, 8034-50.

[12] SS Kulkarni, S Mathad, U Khadke and AH Patil. Dielectric spectroscopy of ferroelectric crossbred PVDF-ZnO polymer composite thin films. *J. Nano Electron. Phys.* 2021; **13**, 4014.

[13] MM Ba-Abbad, AAH Kadhum, AB Mohamad, MS Takriff and K Sopian. Synthesis and catalytic activity of TiO_2 nanoparticles for photochemical oxidation of concentrated chlorophenols under direct solar radiation. *Int. J. Electrochem. Sci.* 2012; **7**, 4871-88.

[14] K Thamaphat, P Limsuwan and B Ngotawornchai. Phase characterization of TiO2 powder by XRD and TEM. *Kasetsart J.* 2008; **42**, 357-61.

[15] HP Klug and LE Alexander.*X-ray diffraction procedures for polycrystalline and amorphous materials*. Wiley, New York, 1997.
[16] X Cai, T Lei, D Sund and L Lin. A critical analysis of the α, β and γ phases in poly(vinylidene fluoride) using FTIR. *RSC Adv.* 2017; **7**, 15382-9.
[17] PI Devi and K Ramachandran. Dielectric studies on hybridised PVDF-ZnO nanocomposites. *J. Exp. Nanoscience* 2011; **6**, 281-93.
[18] ABDNandiyanto, ROktiani, RRagadhita.How to read and interpret FTIR spectroscope of organicmaterial. *Indonesian J. Sci. Tech.* 2019; **4**, 98-118.
[19] A Muzaffar, MB Ahamed, K Deshmukh and SKK Pasha. Dielectric properties and electromagnetic interference shielding studies of nickel oxide and tungsten oxide reinforced polyvinylchloride nanocomposites. *Polymer Plast. Tech. Mater.* 2020; **50**, 1667-78.
[20] N Joseph and MT Sebastian.Electromagnetic interference shielding nature of PVDF-carbonyl iron composites. *Mater. Lett.* 2013; **90**, 64-7.
[21] WM Xia and ZC Zhang. PVDF-based dielectric polymers and their applications in electronic materials. *IET Nanodielectr* 2018; **1**, 17-31.